Check for updates

View Article Online
View Journal

PCCP

Accepted Manuscript

This article can be cited before page numbers have been issued, to do this please use: F. J. J. Martinez-Casado, M. Ramos Riesco, J. A. Cheda, M. I. Redondo Yélamos, L. Garrido, A. Fernandez-Martinez, J. García-Barriocanal, I. da Silva, M. A. Duran-Olivencia and A. Poulain, *Phys. Chem. Chem. Phys.*, 2017, DOI: 10.1039/C7CP02351K.

This is an Accepted Manuscript, which has been through the Royal Society of Chemistry peer review process and has been accepted for publication.

Accepted Manuscripts are published online shortly after acceptance, before technical editing, formatting and proof reading. Using this free service, authors can make their results available to the community, in citable form, before we publish the edited article. We will replace this Accepted Manuscript with the edited and formatted Advance Article as soon as it is available.

You can find more information about Accepted Manuscripts in the author guidelines.

Please note that technical editing may introduce minor changes to the text and/or graphics, which may alter content. The journal's standard Terms & Conditions and the ethical guidelines, outlined in our author and reviewer resource centre, still apply. In no event shall the Royal Society of Chemistry be held responsible for any errors or omissions in this Accepted Manuscript or any consequences arising from the use of any information it contains.

ROYAL SOCIETY OF CHEMISTRY

rsc.li/pccp

View Article Online
DOI: 10.1039/C7CP02351K

PCCP

ARTICLE

Lead(II) Soaps: Crystal Structures, Polymorphism, Solid and Liquid Mesophases

Received 00th January 20xx,
Accepted 00th January 20xx

DOI: 10.1039/x0xx00000x

www.rsc.org/

F. J. Martínez-Casado,*[a] M. Ramos-Riesco,[b] J. A. Rodríguez-Cheda,[b] M. I. Redondo-Yélamos,[b] L. Garrido,[c] A. Fernández-Martínez,[d] J. García-Barriocanal,[e] I. da Silva,[f] M. Durán-Olivencia,[g] A. Poulain.[h]

The long-chain members of lead(II) alkanoates series or soaps, from octanoate to octadecanoate, have been thoroughly characterized by means of XRD, PDF-Analysis, DSC, FTIR, ssNMR and other techniques, in all their phases and mesophases. The crystal structures at room temperature of all the members of the series are now solved, showing the existence of two polymorphic forms in the room temperature crystal phase, different for short and long-chain members. Only nonanoate and decanoate present both forms, and this polymorphism is proven to be monotropic. At higher temperature, these compounds present a solid mesophase, defined as rotator, a liquid crystal phase and a liquid phase, all of them with a similar local arrangement. Since some lead(II) soaps appear as degradation compounds in oil paintings, the solved crystal structures of lead(II) soaps can now be used as fingerprints for their detection by X-ray diffraction. Pair Distribution Function Analysis on these compounds are very similar in the same phases and mesophases for the different members, showing the same short range order. This observation suggests that this technique could also be used in the detection of these compounds in disordered phases or in the initial stages of formation in paintings.

.

Introduction

Pure metal n-alkanoates or soaps have been largely studied for their physicochemical properties,[1-5] derived from their structure, which makes them present tendency to form ionic liquid crystal phases and other mesophases. In particular, lead(II) soaps with medium and large chain length,[6-13] were intensively analysed mainly due to their low temperature thermotropic ionic liquid crystal phase, as well as the short chain members, which are not mesogens but easily quench into different glass states,[14-16] or decompose as in the case of lead(II) acetate.[17]

The main physicochemical feature of this series $Pb(Cn)_2$ from now on, where n is the total number of carbons of the alkanoate group) is the presence of *polymesomorphism*:[18] there is a first transition from a completely ordered crystal at RT (S*II*) to a solid mesophase (S*I*), that we identified as a *rotator* phase,[13] and secondly followed by a fusion to a liquid crystal (*neat phase* or *smectic A-like*), which thirdly melts into a stable isotropic liquid (ionic) at the *clearing* point. Besides the polymesomorphism (*rotator* and *smectic A-like*), we prove in this work, that some members of this series present as well monotropic *polymorphism*. This property has been recently discovered in other metal soaps, like copper(II) alkanoates[19] or lithium acetate.[20] Apart from this, the crystal structure of long-chain lead(II) soaps is also given here for the first time, since, until now, only the ones of short and medium members were solved.[16,17,21-23]

Lead(II) exhibits intense optical properties, showing luminescence in 3D-coordination polymers,[24] including some lead(II) butyrate-based compounds,[25] which show potential application as X-ray phosphors and luminescent materials in light-emitting devices.[17] More surprisingly, pure lead(II) soaps (2D coordination polymers) present weak fluorescence in the

[a] *MAX IV Laboratory, Lund University, Fotongatan 2, SE-225 94 Lund, Sweden. E-mail: francisco.martinez@maxiv.lu.se*
[b] *Dpto. Química Física, Facultad de C. Químicas. Universidad Complutense, 28040 Madrid, Spain*
[c] *Dpto. Química Física, Instituto de Ciencia y Tecnología de Polímeros, CSIC, 28006 Madrid, Spain*
[d] *CNRS & Univ. Grenoble Alpes, ISTerre, F-38041 Grenoble, France*
[e] *Univ. Minnesota, Characterizaterization Facility, Minneapolis, MN 55455 USA*
[f] *ISIS Facility, Rutherford Appleton Laboratory, Harwell Oxford, Didcot OX11 0QX, United Kingdom*
[g] *Department of Chemical Engineering, Imperial College London, United Kingdom*
[h] *ESRF, F-38043 Grenoble, France*

† Electronic Supplementary Information (ESI) available:. Crystallographic information files (cif, 16 in total) of $Pb(C8)_2$ (CCDC-1473674, at 100 K), $Pb(C9)_2$ *polymorph A* (CCDC-1473675, at 298 K), $Pb(C10)_2$ *polymorph A* (CCDC-1473676, at 298 K), solved by SCXRD, and $Pb(C8)_2$ (CCDC-1473677, at 298 K), $Pb(C9)_2$ *polymorph A* (CCDC-1473795, at 298 K), $Pb(C9)_2$ *polymorph B* (CCDC-1473796, at 298 K), $Pb(C10)_2$ *polymorph A* (CCDC-1473684, at 298 K), $Pb(C10)_2$ *polymorph B* (CCDC-1473685, at 298 K), $Pb(C11)_2$ (CCDC-1473797, at 298 K), $Pb(C12)_2$ (CCDC-1473683, at 298 K), $Pb(C13)_2$ (CCDC-1473686, at 298 K), $Pb(C14)_2$ (CCDC-1473687, at 298 K), $Pb(C15)_2$ (CCDC-1473688, at 298 K), $Pb(C16)_2$ (CCDC-1473689, at 298 K), $Pb(C17)_2$ (CCDC-1473690, at 298 K), and $Pb(C18)_2$ (CCDC-1473691, at 298 K), solved by HRPD. For ESI and crystallographic data in CIF or other electronic format see DOI: 10.1039/x0xx00000x
In the Supporting Information file: Thermal data (transition temperatures, enthalpies and entropies, from DSC), Rietveld refinement fittings, FTIR data, ssNMR data (C-13 and Pb-207), and Electric Spectroscopy data.

Published on 07 June 2017. Downloaded by State University of New York at Binghamton on 07/06/2017 16:49:10.

Physical Chemistry Chemical Physics Accepted Manuscript

Please do not adjust margins

View Article Online
DOI: 10.1039/C7CP02351K

Published on 07 June 2017. Downloaded by State University of New York at Binghamton on 07/06/2017 16:49:10.

crystal phase at low temperature,[26] but strong phosphorescence in the glass states (from lead(II) propionate to heptanoate) even at room temperature.[16] On the other hand, lead(II) soaps might as well be potential candidates to prepare glassy composites, which can be prepared using mesomorphic metal alkanoates and that have been proven to behave as non-linear optics materials.[27,28]

Besides all these remarkable properties, the relevance of lead(II) soaps has grown hugely in the last two decades, because they were found as degradation products in historical oil paintings (detected for the first time in Rembrandt's masterpiece *The Anatomy Lesson of Dr. Nicolaes Tulp*)[29] in the form of *protrusions* which deteriorate the painting.[30] Since then, not only lead soaps, but also of other metals (*e.g.*, Zn, Cu(II), K, etc.)[31-33] were found, creating several and diverse problems in the conservation of artworks. Metal soaps appear due to the reaction between the pigments or drier agents (for instance, *white lead* or *litharge*, respectively) with fatty acids formed from the hydrolysis of the binding linseed oil (consisting in a mixture of triglycerides esters of large fatty acids and glycerin).[31,34-37] The lead(II) soaps that are mainly detected are lead(II) hexadecanoate or palmitate, octadecanoate or stearate, or others from unsaturated acids (oleate, linoleate, linolenate). The detection of lead and other metal soaps in paintings is carried out typically by infrared spectroscopy or diffraction. But, since they are compared to standards for frequencies or *d*-spacings, respectively, it is difficult to detect them in the shape of nanocrystals, non-crystalline or partially disordered phases, or in the early stages of formation, although amorphous lead carboxylates have been detected by FTIR recently.[32,38] For that, we propose the use of techniques which focus in the local ordering, such as Pair Distribution Function (PDF) Analysis or X-ray Absorption. Thus, the crystal structures and the PDF curves (of the different phases and mesophases) given in this work may be used as *fingerprints* in the detection of lead(II) soaps in the crystal form and in any other phase or mesophase, respectively.

Experimental

Sample Preparation

The method of synthesis consists in the metathesis of the potassium ion from the corresponding alkanoate in absolute ethanol solution, by the lead(II) ion, added as nitrate, dissolved in a small amount of water, followed by at least two recrystallizations in benzene.[10] The chemicals used for the synthesis are specified in the Supplementary Information (Table S1). The purity of the synthesized salts was assessed by differential scanning calorimetry (DSC), with values higher than 99.5 %.

Crystals of $Pb(C8)_2$, $Pb(C9)_2$-A and $Pb(C10)_2$-A, suitable for X-ray studies were grown by counter diffusion in agarose gel in U tubes, from aqueous solutions of 50 mM of $Pb(NO_3)_2$ and 100 mM of the corresponding sodium alkanoate (alkanoic acid + NaOH). The sizes of the single crystals used in the SCXRD experiments are given in Table 1, for all of the samples. In the case of the $Pb(C10)_2$, crystals of polymorph B were also found in the U tube mixed with $Pb(C10)_2$-A, with poor quality, sufficient enough to solve the structure and obtain a model but yielding poor statistics. Thus, the structure of $Pb(C10)_2$-B was solved by High Resolution Powder Diffraction (HRPD) using the aforementioned model.

Single Crystal X-ray Diffraction (SCXRD)

Measurements for $Pb(C8)_2$ were conducted using synchrotron radiation (with λ = 0.7379 Å) at the BM16 Spanish beamline of ESRF with a CCD detector (ADSCq210rCCD), making phi scans when collecting the data. The oscillation range ($\Delta\varphi$) used for each image was one degree. The compound was measured at 100 K. Diffraction data for anhydrous $Pb(C9)_2$-A and $Pb(C10)_2$-A were collected on a Bruker APEXII CCD diffractometer equipped with graphite-monochromated Cu-Kα radiation with radiation wavelength 1.54178 Å, by using the *phi-omega* scan technique at 296 K.

The experimental parameters, crystal size, and main crystallographic data for $Pb(C8)_2$, $Pb(C9)_2$-A and $Pb(C10)_2$-A are shown in Table 1.

Table 1. Experimental parameters and main crystallographic data for the compounds studied by single crystal XRD.

Data	$Pb(C8)_2$	$Pb(C9)_2$ polymorph A	$Pb(C10)_2$ polymorph A
Empirical Formula	$PbC_{16}H_{30}O_4$	$PbC_{18}H_{34}O_4$	$PbC_{20}H_{38}O_4$
Mr (g·mol^{-1})	493.59	*521.64*	549.69
Crystal system	Triclinic	Triclinic	Triclinic
Space group (No.)	*P-1* (2)	*P*-1 (2)	*P*-1 (2)
Crystal size (mm)	0.080 × 0.030 × 0.010	0.120 × 0.100 × 0.050	0.150 × 0.100 × 0.040
λ (Å)	0.73790	1.54178	1.54178
Temperature (K)	100(2)	298(2)	298(2)
a (Å)	4.788(1)	4.8937(2)	4.910(5)
b (Å)	7.1940(14)	7.3246(3)	7.327(5)
c (Å)	25.648(5)	28.2872(13)	30.806(5)
α (°)	87.63(3)	91.643(2)	88.565(5)
β (°)	85.55 (3)	94.767(2)	85.855(5)
γ (°)	89.31 (3)	90.710(2)	89.391(5)
V (Å^3)	880.0(3)	1009.90(7)	1105.0(14)
Z	2	2	2
D_c (g·cm^{-3})	1.863	1.715	1.652
μ (mm^{-1})	9.60	16.369	14.994
Absorption correction	multi-scan	multi-scan	multi-scan
Reflection collected	3775	3370	3734
Reflections with I > 2σ(I).	3633	3179	3420
Parameters refined /restrains	191 / 0	208 / 0	227 / 0
Hydrogen treatment	not refined	not refined	not refined
R-factor	0.0738 / 0.1778	0.0652	0.0465
wR2-factor	0.0746 / 0.1808	0.1769	0.1086
Goodness of fit	1.052	1.093	1.100
CCDC deposition numbers	1473674	1473675	1473676

The structures were solved by direct methods and subsequent Fourier syntheses using the SHELXS-97 program,[39] and were refined by the full-matrix least-squares technique against F^2,

Physical Chemistry Chemical Physics Accepted Manuscript

This journal is © The Royal Society of Chemistry 20xx

Please do not adjust margins

View Article Online
DOI: 10.1039/C7CP02351K
PCCP ARTICLE

Published on 07 June 2017. Downloaded by State University of New York at Binghamton on 07/06/2017 16:49:10.

using the SHELXL-97 program. Anisotropic thermal parameters were used to refine all non-H atoms. Hydrogen atoms were placed in idealized positions, and their parameters were not refined. A semi-empirical absorption correction ('multi-scan') was done for these compounds, due to the presence of heavy atoms.

Powder X-ray Diffraction

HRPD measurements were performed on all the compounds, from $Pb(C8)_2$ to $Pb(C18)_2$. In the case of $Pb(C8)_2$, it was measured at room temperature to confirm the structure solved by SCXRD (at 100 K). The structures of $Pb(C9)_2$-B and $Pb(C10)_2$-B were solved from mixtures of polymorphs A and B, where polymorphs A were solved by SCXRD in both cases.

$Pb(C8)_2$ and the mixture of $Pb(C10)_2$-A and B were measured at RT in transmission mode in 0.5 mm spinning capillaries at the I711 beamline of Max II synchrotron (MAX IV Laboratory, Lund, Sweden), with a wavelength of 0.9941 Å, and using a Newport diffractometer equipped with a Pilatus 100K area detector mounted 76.5 cm from the sample. The detector was scanned continuously, from 2 to 70° (for $Pb(C8)_2$) and from 0 to 60° (for the mixture of $Pb(C10)_2$), in approx. 6-10 min, recording 125 images/° (step size 0.008°) for each measurement. The true 2-theta position of each pixel was recalculated, yielding an average number of 100000 pixels contributing to each 2Θ value. Integration, applying no corrections for the tilt of the detector, provided FWHM values of 0.03-0.08° from 0 to 120°. Measurements in the S*I* phase (high temperature) for all the compounds were also carried out using this set-up and controlling the temperature (from 285 to 410 K) with an Oxford Cryojet5.

Measurement for $Pb(C12)_2$ was conducted at RT using synchrotron radiation (with λ = 0.8266 Å) at the SpLine beamline (BM25) at the European Synchrotron Radiation Facility (ESRF, Grenoble), using a 0.7 mm spinning capillary, from 0.5° to 50° and in a 2θ-step scan mode with 0.015° step and 3-5 sec. acquisition time per point.

The mixture of polymorphs of $Pb(C9)_2$-A and B and the rest of the compounds, $Pb(C11)_2$ and $Pb(C13)_2$-$Pb(C18)_2$, were measured at RT in transmission mode in a Panalytical X'Pert PRO diffractometer equipped with a focusing mirror and a fast detector X'Celerator (Cu Kα1 radiation, 40 kV, 45 mA). The measurement ranges of 2θ were from 2° to 90°, for $Pb(C9)_2$ (step size 0.008°) and from 1° to 90° for the rest of the compounds (step size 0.017°). The samples were prepared in 0.5 mm-diameter glass capillaries, and rotated during exposure.

The Rietveld refinement was performed with the *FullProf*[40,41] program, introducing the atomic coordinates previously obtained from the single crystal data in each case. The main experimental parameters and crystallographic data are shown in Tables 2 (from $Pb(C8)_2$ to $Pb(C10)_2$) and 3 (from $Pb(C11)_2$ to $Pb(C18)_2$). The fitting curves for all the compounds are given in the Supporting information (Figures S3 and S4).

Table 2 Experimental parameters and main crystallographic data for $Pb(C8)_2$, and the mixtures of polymorphs (A and B) of $Pb(C9)_2$ and $Pb(C10)_2$.

Crystal data	*Pb(C8)₂*	*Pb(C9)₂* *Mixture of polymorphs A + B*		*Pb(C10)₂* *Mixture of polymorphs A + B*	
		polymorph A	polymorph B	polymorph A	polymorph B
Empirical Formula	$PbC_{16}H_{30}O_4$	$PbC_{18}H_{34}O_4$		$PbC_{20}H_{38}O_4$	
Mr (g·mol^{-1})	493.59	521.64		549.69	
Cell setting, space group (no.)	Triclinic, *P-1* (2)	Triclinic, *P-1* (2)	Monoclinic, *P2/c* (13)	Triclinic, *P-1* (2)	Monoclinic, *P2/c* (13)
a (Å),	4.86902(3)	4.89365	54.9422(3)	4.8865(4)	60.021(2)
b (Å)	7.30619(5)	7.32459	4.98011(10)	7.2966(6)	4.9611(2)
c (Å)	25.6951(2)	28.2414(12)	7.25685(16)	30.7267(14)	7.2496(4)
α (°)	88.1812(8)	91.64034	90.00000	88.630(11)	90.00000
β (°)	85.2246(7)	94.75932	90.5625(15)	85.856(10)	90.272(8)
γ (°)	89.1022(7)	90.71046	90.00000	89.552(16)	90.00000
Volume (Å^3)	910.369(12)	1008.27(4)	1985.51(6)	1092.36(14)	2158.68(18)
Z, D_c (g·cm^{-3})	2, 1.785	2, 1.718	4, 1.745	2, 1.672	4, 1.692
Diffractometer	I711 (MAX IV Lab.)	PANalytical XPERT-PRO		I711 (MAX IV Laboratory)	
Wavelength (Å)	0.9941	Cu $Kα_1$		0.9941	
Temperature (K)	298(2)	298(2)		298(2)	
2θ range (°), step size (° 2θ)	2-70, 0.008	2-90, 0.008		0.015-60, 0.008	
R_p, R_{wp}, R_{exp}	0.0681, 0.1032, 0.0761	0.0827, 0.1162, 0.0268		0.0636, 0.0913, 0.022	
Goodness-of-fit	1.39	4.33		3.52	
No. of parameters	98	115		19	
No. of contributing reflections	3494	3543	3602	4549	2707
R_F, R_{BRAGG}	0.0185, 0.0400	0.0292, 0.0895	0.0304, 0.0434	0.0228, 0.0597	0.0290, 0.0636
Mass fraction (%)	100	7.5	92.5	61.0	39.0
CCDC deposition number	1473677	1473795	1473796	1473684	1473685

Physical Chemistry Chemical Physics Accepted Manuscript

Please do not adjust margins

View Article Online
DOI: 10.1039/C7CP02351K

PCCP

ARTICLE

Published on 07 June 2017. Downloaded by State University of New York at Binghamton on 07/06/2017 16:49:10.

Physical Chemistry Chemical Physics Accepted Manuscript

Routine XRD measurements as a function of temperature were carried out in reflection mode with a Panalytical X'Pert PRO MPD X-ray diffractometer with vertical goniometer θ/θ and RTMS X'Celerator detector equipped with a high-temperature camera Anton Paar HTK1200 (Cu Kα1 radiation, 1.54056 Å, 45 kV, 40 mA, Ni filter). In-situ XRPD scans were measured in inert atmosphere ($N_{2(g)}$) from 2θ = 2-40° at several temperatures in the range from 298 to 393 K during heating and cooling, after programming every temperature change at a rate of 3 K·min^{-1}.

High-energy Total X-ray Scattering and PDF Analysis.

Finely powdered dry samples were loaded into 1.0 mm diameter kapton capillaries. High-energy X-ray total scattering data acquisition was performed at beamline ID31, at the ESRF. Scattering data were collected at different temperatures with a flat panel Perkin Elmer using the Rapid-Acquisition Pair Distribution Function technique.[42] Samples, an empty capillary and the background were measured at RT from 1–25.0 Å^{-1}. The X-ray wavelength was refined using a CeO_2 standard (λ = 0.17844 Å). Corrections for sample-detector distance, tilt angle of the detector with respect to the direction of the incident radiation and polarization were performed using Fit2D.[43] Total scattering structure factors and PDFs were obtained using the PDFGetX3 software.[44]

Differential Scanning Calorimetry (DSC)

A TA Instruments DSC Model Q10 was used in this work. Tightly sealed aluminum volatile pans (in N_2 atmosphere) were used to scan at different heating rates (in dry nitrogen atmosphere at a gas flow of about 50 mL·min^{-1}). An MT5 Mettler microbalance was used to weigh the about 10 mg samples (error: ± 0.001 mg). The calorimeter was calibrated for temperature using standard samples of In and Sn, supplied by TA (purity > 99.999 % and > 99.9 %, respectively), and of benzoic acid (purity > 99.97 %), supplied by the former NBS (lot 39i), and for enthalpy using the standards of In and Sn.

FTIR spectroscopy.

Infrared spectra of samples in KBr pellets were recorded using a Nicolet Magna 750 FTIR spectrometer at a resolution of 2 cm^{-1}. A commercial variable temperature cell, SPECAC VTL-2, adapted for solid samples, was employed to obtain IR spectra of the heated samples.

Table 3 Experimental parameters and main crystallographic data for compounds from $Pb(C11)_2$ to $Pb(C18)_2$ (all of them with the polymorph B structure)

Crystal data	$Pb(C11)_2$	$Pb(C12)_2$	$Pb(C13)_2$	$Pb(C14)_2$	$Pb(C15)_2$	$Pb(C16)_2$	$Pb(C17)_2$	$Pb(C18)_2$
Empirical Formula	$PbC_{22}H_{42}O_4$	$PbC_{24}H_{46}O_4$	$PbC_{26}H_{50}O_4$	$PbC_{28}H_{54}O_4$	$PbC_{30}H_{58}O_4$	$PbC_{32}H_{62}O_4$	$PbC_{34}H_{66}O_4$	$PbC_{36}H_{70}O_4$
Mr (g·mol^{-1})	577.76	605.81	633.86	661.91	689.98	718.02	746.07	774.14
Cell setting, space group (no.)	Monoclinic, *P2/C* (13)	Monoclinic, *P2/C* (13)	Monoclinic, *P2/C* (13)	Monoclinic, *P2/C* (13)	Monoclinic, *P2/C* (13)	Monoclinic, *P2/C* (13)	Monoclinic, *P2/C* (13)	Monoclinic, *P2/C* (13)
a (Å),	65.1516(9)	70.263(2)	75.2787(17)	80.5448(19)	85.4764(13)	90.6159(13)	95.649(2)	100.847(2)
b (Å)	4.9710(7)	4.96672(15)	4.96255(12)	4.96393(16)	4.96236(12)	4.96125(11)	4.9544(2)	4.9589(2)
c (Å)	7.2708(1)	7.2705(2)	7.2836(2)	7.2966(3)	7.2959(2)	7.30027(18)	7.2989(4)	7.3030(4)
β (°)	90.498(3)	90.564(3)	90.581(3)	90.514(3)	90.590(3)	90.463(3)	90.492(6)	90.488(4)
Volume (Å^3)	2354.73(3)	2537.09(1)4)	2720.83(1)2)	2917.22(1)6)	3094.50(1)3)	3281.86(1)2)	3458.7(3)	3652.0(2)
Z, D_c (g·cm^{-3})	4, 1.630	4, 1.586	4, 1.547	4, 1.507	4, 1.481	4, 1.453	4, 1.433	4, 1.408
Wavelength (Å)	Cu $K\alpha_1$	0.8266	Cu $K\alpha_1$	Cu $K\alpha_1$	Cu $K\alpha_1$	Cu $K\alpha_1$	Cu $K\alpha_1$	Cu $K\alpha_1$
Temperature (K)	298(2)	298(2)	298(2)	298(2)	298(2)	298(2)	298(2)	298(2)
2θ range (°), step size (° 2θ)	1-90, 0.017	0.5-50, 0.015	1-90, 0.017	1-90, 0.017	1-90, 0.017	1-90, 0.017	1-90, 0.017	1-90, 0.017
R_p, R_{wp}, R_{exp}	0.0773, 0.1133, 0.0287	0.0451, 0.0671, 0.0279	0.0821, 0.1272, 0.0214	0.1062, 0.1563, 0.0213	0.0692, 0.1106, 0.0568	0.0469, 0.0790, 0.0196	0.0925, 0.1643, 0.0194	0.0888, 0.1645, 0.0139
R_F, R_{BRAGG}	0.0271, 0.0671	0.0414, 0.0654	0.0345, 0.0767	0.0628, 0.0725	0.0592, 0.0524	0.0302, 0.0324	0.0514, 0.0611	0.0232, 0.0448
Goodness-of-fit	4.04	2.40	5.94	7.35	1.95	3.88	8.47	8.07
No. contributing reflections	4524	3488	5145	5268	5523	6202	6270	6618
No. parameters	82	69	13	16	10	14	13	86
CCDC deposition number	1473797	1473683	1473686	1473687	1473688	1473689	1473690	1473691

Please do not adjust margins

View Article Online
DOI: 10.1039/C7CP02351K
PCCP ARTICLE

Published on 07 June 2017. Downloaded by State University of New York at Binghamton on 07/06/2017 16:49:10.

C-13 and Pb-207 CP/MAS NMR.

Solid state C-13 and Pb-207 NMR measurements were performed in a Bruker Avance™ 400 spectrometer (Bruker BioSpin GmbH, Rheinstetten, Germany) equipped with a 89 mm wide bore, 9.4 T superconducting magnet (C-13 and Pb-207 Larmor frequencies at 100.61 and 83.71 MHz, respectively). Powdered samples were placed in 4 mm zirconia rotors (about 60 mg of sample). All reported data were acquired at two temperatures, first at (296 ± 0.1) K and then after thermal equilibrium was reached at a temperature corresponding to the S*I* phase (ranging aprox. 370-380 K, with a precision of ± 0.1 K). We used a standard Bruker double resonance 4 mm cross-polarization (CP)/magic angle spinning (MAS) NMR probe head using a 90° C-13 pulse length of 4.2 µs. The C-13 spectra were acquired with 1 ms CP contact time, 5 s recycle delay, MAS spinning rates of 6.5 kHz and 1000 transients. High-power proton decoupling of 75 kHz was used. The NMR spectra were evaluated with the spectrometer manufacture's software package Topspin™. All free-induction decays were subjected to standard Fourier transformation with 5 Hz line broadening and phasing. The chemical shifts were externally referenced to adamantane (29.5 ppm) secondary to TMS (0.0 ppm).

The Pb-207 NMR spectra were acquired with 4 ms CP contact time, 10 s recycle delay, MAS spinning rates of between 4.0 and 9.0 kHz and 3000 to 12000 transients. High-power proton decoupling of 75 kHz was used and the NMR spectra were also evaluated with Topspin™. All free-induction decays were subjected to standard Fourier transformation with 400 Hz line broadening and phasing. The chemical shifts were externally referenced to tetra-phenyl-lead (IV) (-135 ppm).[45]

Results and discussion

Crystal structures and polymorphism (solid phase S*II*)

The S*II* phase in lead(II) soaps is the crystalline phase at room temperature. However, this generically called S*II* phase consists actually in two different polymorphic forms from the short to the long members of the series. This polymorphism was already suspected in previous studies (see Supp. Info., Figure S24)[46] and it is confirmed here.

The crystal structures in the S*II* phase of all the compounds from $Pb(C8)_2$ to $Pb(C18)_2$ have been solved and refined here, being only $Pb(C9)_2$-B reported recently,[47] from these salts. The main aspect of this crystallographic study, as mentioned before, is the existence of two different polymorphs in the lead(II) alkanoates series in their crystal phase (S*II*): A, from $Pb(C2)_2$ to $Pb(C10)_2$, and B, from $Pb(C9)_2$ to $Pb(C18)_2$. Only $Pb(C9)_2$ and $Pb(C10)_2$ present both polymorphic phases.

Both polymorphs, A and B, show a lamellar structure forming a 2D coordination polymer, with one Pb atom and two alkyl chains in the asymmetric unit. For both as well, the alkyl chains present an *all-trans* conformation, and the planes formed by the C atoms in the hydrocarbon chains (*all-trans*) are arranged with a *herring-bone* structure (*internal orientational* order).[18]

However, the main difference between them lies in the coordination of the Pb atoms: *hemidirected* (with the O atoms directed throughout one hemisphere of the coordination sphere) and *holodirected* (with the O atoms more regularly situated around the Pb atom).

Polymorph A shows two types of carboxylates: (a) a μ_2-$\eta^2\eta^1$ carboxylate (with both O atoms chelating one Pb atom and one of them also coordinating another Pb) and (b) a μ_3-$\eta^2\eta^2$ carboxylate (with both oxygens bridging and chelating). The coordination number of lead(II) is seven, with the O atoms forming a distorted monocapped trigonal prism, with a *hemidirected* geometry. This polymorph appears in the short lead(II) soaps ($Pb(C2)_2$-$Pb(C7)_2$ already reported),[16,17,21,22] and present a monoclinic unit cell ($P2_1/m$) for $Pb(C2)_2$-$Pb(C4)_2$, and triclinic (P-1) for $Pb(C5)_2$-$Pb(C10)_2$ (see Figure 1a).

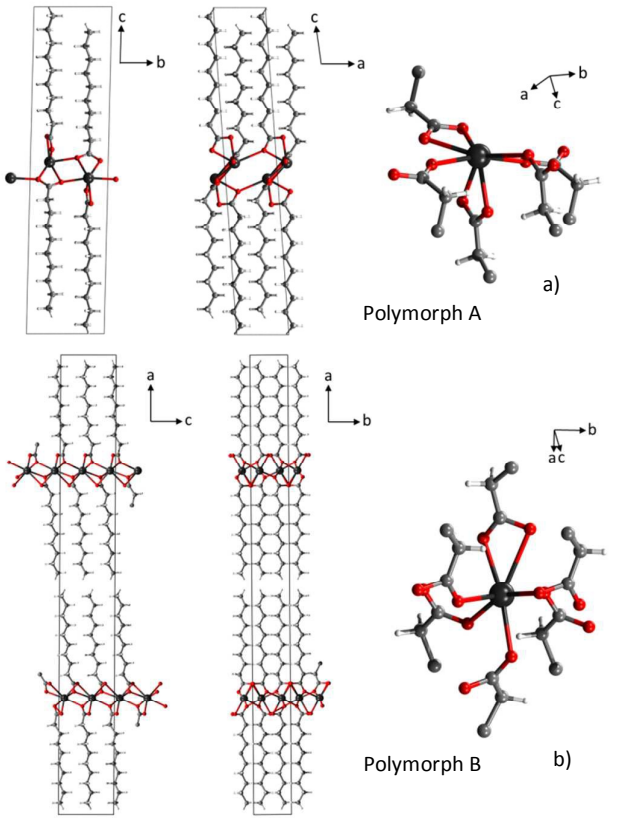

Fig. 1 Crystal structures of polymorphs A (a) and B (b) of $Pb(C10)_2$, represented in the indicated directions and showing the coordination of the Pb atoms in both cases (hemidirected and holodirected, respectively).

On the other hand, polymorph B presents a monoclinic cell ($P2/c$) with a doubled long cell parameter (two bilayers per cell), with respect to polymorph A. The two carboxylates are (a) a μ_3-$\eta^2\eta^1$ carboxylate (with both O atoms bridging) and (b) a μ_3-$\eta^2\eta^2$ carboxylate (with both oxygens bridging and chelating). The coordination is seven as well but, in this case, with a pentagonal bipyramidal geometry around the Pb atom (*holodirected*) (see Figure 1b). This new polymorphic phase

Physical Chemistry Chemical Physics Accepted Manuscript

Please do not adjust margins

View Article Online
DOI: 10.1039/C7CP02351K

Published on 07 June 2017. Downloaded by State University of New York at Binghamton on 07/06/2017 16:49:10.

Physical Chemistry Chemical Physics Accepted Manuscript

was first reported by Catalano *et al.* for $Pb(C9)_2$-B, studying as well the different coordination of the Pb atoms by ssNMR.[23,47] C-13 and Pb-207 ssNMR measurements were also carried out here for $Pb(C10)_2$, $Pb(C11)_2$, $Pb(C14)_2$, and $Pb(C15)_2$ (see Supp. Info., Figures S17 to S23, and Tables S6 and S7). The C-13 results show that in the *SII* phase, two carboxylates and only one signal from the methyl groups are observed (there are two kinds from the crystallographic point of view but with similar environment and indistinguishable by NMR), as it could be expected for polymorph B,[23] with the exception of $Pb(C10)_2$ showing a more complex (higher multiplicity of resonances) C-13 spectrum. It is noteworthy highlighting that three carboxylate (C1) peaks at 184.9, 184.2 and 183.8 are observed and, also, the methyl group (C10) shows two peaks at 15.5 and 15.1 ppm (see Supp. Info., Figure S17), implying a mixture of polymorphs A and B may be present this sample.[23]

Pb-207 ssNMR spectra of these alkanoates show isotropic chemical shifts, δ_{iso}, between -2136 and -2114 ppm (Figs. S18, S21, S23 and Table S7, in Supp. Info.), lower values than those observed in polymorphs A and suggesting longer Pb-O bond lengths in polymorphs B, as indicated earlier. Also, a small span, Ω = 702-675 ppm, that is characteristic of a holodirected coordination geometry is observed.[23,47]

The PDFs of both kinds of polymorphs show clear differences, especially in the Pb-O and Pb-Pb distances, as expected from the different coordination environments and arrangement of Pb atoms. On the other hand, the PDFs of the same polymorph in different members are similar in the short-medium range (for distances smaller than the stacking of layers; that is, the long *d*-spacing). This is shown in Figure 2 for polymorph A ($Pb(C7)_2$ and $Pb(C8)_2$) and B ($Pb(C9)_2$, $Pb(C10)_2$ and $Pb(C11)_2$).

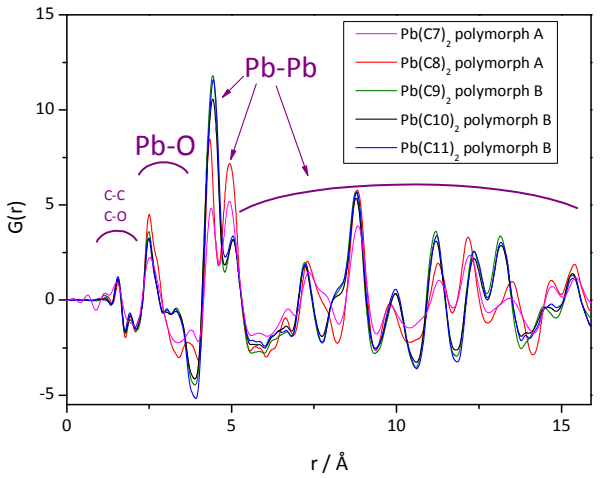

Fig. 2 Pair Distribution Function (PDF) analysis of high-energy X-ray total scattering data for $Pb(C7)_2$, $Pb(C8)_2$, $Pb(C9)_2$, $Pb(C10)_2$ and $Pb(C11)_2$ on the S*II* phase (RT) in the indicated polymorphic phase. The data for $Pb(C7)_2$ is taken from reference 16).

$Pb(C9)_2$ and $Pb(C10)_2$ present both polymorphic forms, A and B, and in both cases, the latter is the stable one. Depending on the route used, the different polymorphs or mixtures of them can be obtained. Thus, for $Pb(C9)_2$, polymorph B is favoured in the synthesis explained above, sometimes obtained almost pure or in mixtures with high ratio of B (A:B ratio of 7:93 or higher in B, with this route). In the case of $Pb(C10)_2$, a mixture of an approx. 1:9 ratio is obtained, using the aforementioned synthesis. On the other hand, cooling from the melt, the ratio of polymorphs A increases (approx. 4:6 and 6:4 for $Pb(C9)_2$ and $Pb(C10)_2$, respectively), being almost the only crystal phase when the quenching process is fast enough (9:1 and almost 1:0, respectively, at cooling rates higher that 50 $K \cdot min^{-1}$). The effect of a heating-cooling cycle 296-365-296 K on the appearance of C-13 ssNMR spectra of $Pb(C10)_2$ is shown in Fig. S17 (Supp. Info.). The variation in intensity of the carboxylate and methyl peaks between the spectra collected at 296 K, before and after heating, suggests a change in the sample polymorphs composition. Finally, samples prepared by counter diffusion in gel favour the formation of polymorph A in both cases, although some crystals of B, smaller and of worse quality, were found in the case of $Pb(C10)_2$.

For both $Pb(C9)_2$ and $Pb(C10)_2$, the S*II*-S*I* transition for polymorph B seems to be a complex process and it occurs in two steps, while it happens in a single step for polymorph A. Polymorph B is denser than A for these two compounds, and the final temperatures and enthalpies of the S*II*-S*I* transitions are higher for B, confirming that this is the stable polymorph for $Pb(C9)_2$ and $Pb(C10)_2$. The thermal data (temperatures, enthalpies and entropies) for all the members of the lead soaps series are given in the Supp. Info. (Tables S1 and S2 and Figures S1 and S2).

Intermediate solid phase (S*I*) and fluid phases (LC and IL)

Three different phases exist at high temperature in the lead(II) alkanoates series, besides the crystal phases: the intermediate solid phase (solid *I* or S*I*), the liquid crystal mesophase (LC) and the isotropic liquid phase (IL). S*I* and IL are present for all the members, while the LC phase exist only from $Pb(C6)_2$ to $Pb(C12)_2$, both included.

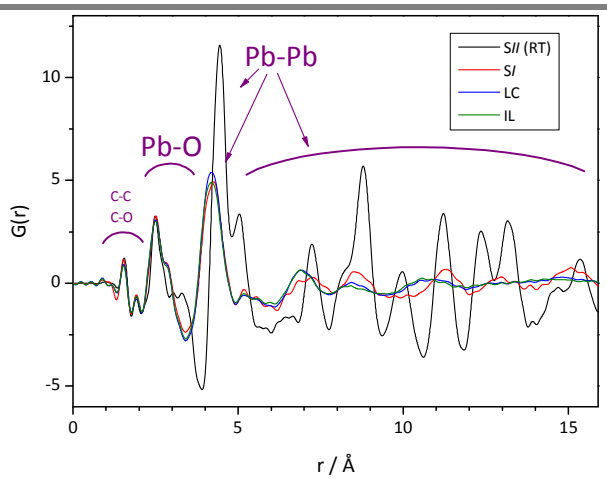

Fig. 3. PDF analysis for the different phases of $Pb(C11)_2$: crystal phase at RT (S*II*, polymorph B), intermediate solid phase (S*I*), liquid crystal (LC) and liquid phase (IL).

The use of complementary techniques, such as diffraction, PDF Analysis, FTIR, ssNMR and optical microscopy allow pointing

This journal is © The Royal Society of Chemistry 20xx

Please do not adjust margins

View Article Online
DOI: 10.1039/C7CP02351K
PCCP ARTICLE

Published on 07 June 2017. Downloaded by State University of New York at Binghamton on 07/06/2017 16:49:10.

out the differences and similarities of these phases. Thus, for instance, diffraction clearly shows the solid and crystalline nature of the S*I* phase while the other two are fluid (few peaks and none for the LC and IL phases, respectively). PDF-Analysis, on the other hand, reveals that the same short range order is common for these three phases (see Figure 3, and Supp. Info., Figures S12 and S13).

1- SI phase (rotator)

This is an crystalline and semi-ordered phase (with positional, external orientation, conformational order)[18], considered a *rotator* phase,[13,15,16] characterized by a high crystallinity, a rotational motion of the alkyl chain (internal orientational disorder),[18] and considerably higher conductivity than the crystal phase (see Supp. Info., Figure S16).[13]

Some of the diffraction patterns in this phase were indexed with the DICVOL06 program[48] (included in the Fullprof Suite) for different members of the series (see Supp. Info. Table S5 and Figure S7), giving possible unit cells with common values for the *a* and *b* parameters: approx. 8.52 and 14.90 Å, respectively. These parameters would correspond to the structure in the layers, as it occurs in the two polymorphs at room temperature with common parameters: approx. 4.9 and 7.3 Å. If we compare the results and consider the unit cells in the SI phase doubled in both axes, the values would be 4.26 and 7.45 Å (×2 in *a* and *b*).

On the other hand, the comparison of the PDFs between the SII and SI phases (see Figure 3) shows similar distances for C-C, C-O and Pb-O distances at short range, and a clear decrease in the Pb-Pb distances: from 4.45(1) to 4.18(1) Å in the first one (from SII to SI). Since the lead(II) soaps contain only Pb, O, C and H atoms, the signal coming from the Pb atoms (much higher Z), especially after the first Pb-Pb peaks appear. To prove this point, a rough fitting was carried out (using the PDFgui program[49]) in the S*II* phase using only Pb atoms and the crystallographic data obtained by XRD, showing a good agreement. Then, a simulation was performed in the S*I* phase, refining the cell parameters and the position of the Pb atoms, obtaining values for *a* and *b* of approx. 4.33 and 7.33 Å, respectively. These values are similar to the aforementioned ones calculated by XRD. At the same time, the refined positions of the Pb atoms in the plane (pseudo-hexagonal) fit the Pb-Pb distances observed in the PDF of the S*I* phase. The fittings for both phases and the calculated arrangement of Pb atoms (in the S*I* phase) are given in the Supporting Information (Figures S11 and S12).

The pseudo-hexagonal arrangement of the Pb atoms would also explain the formation of hexagons observed by optical microscopy when cooling down from the LC to the *SI* phase (see Figure 4).

This hypothetical structure in the S*I* phase explains the shortening of the Pb-Pb distances observed by PDF analysis, with a reduction of the area in the layers (*a* and *b* parameters). On the other hand, the interlayer *d*-spacing observed by XRD decreases as well from the S*II* to the S*I* phase (see Figure S5 in the Supp. Info.). Both results would result in an increase in density from the low to the high temperature solid phase (S*II* to S*I*), which, obviously, does not occur, as it was proven by Bazuin *et al.* by densitometry measurements in $Pb(C10)_2$,[6] and by our group by dilatometry in $Pb(C5)_2$ and $Pb(C9)_2$.[13] However, this apparent paradox could be explained with the *superstructures* studied by Skoulios *et al.* for the high temperature phases in alkaline soaps.[50,51] Thus, these superstructures are formed by the packing of domains (ribbon-like), with a dense arrangement of the polar heads in the central layers of the ribbons and a much less dense packing between ribbons, explaining the overall decrease of density with respect to the crystal phase (see Supp. Info., Figure S25).

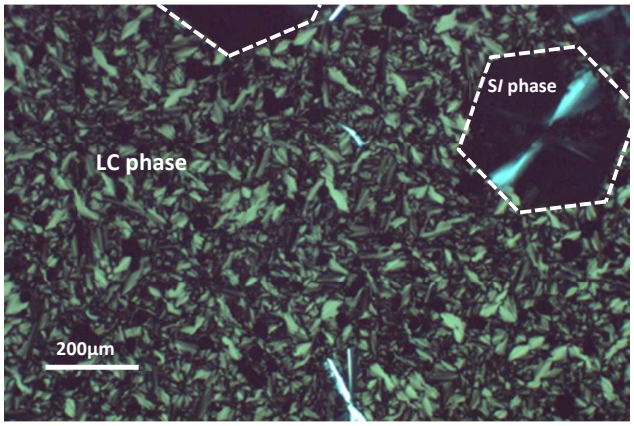

Fig. 4. Formation of hexagonal domains (highlighted) observed by optical microscopy (with crossed polars), corresponding to the formation of the S*I* phase on cooling from the liquid crystal phase.

FTIR and ssNMR reveal interesting and distinctive features of this phase, especially about the methyl and methylene groups and carboxylates of the alkyl chains and the coordination of the heavy atoms. On one hand, infrared spectra show that at the S*II* to S*I* transition temperature only one band at 2960 cm^{-1} is observed for this mode indicating that from this point free rotation of the methyl groups takes place (see Figure 5a). The CH_2 symmetric (υ_{symm}) and asymmetric (υ_{asymm}) stretching bands at 2849 cm^{-1} and 2918 cm^{-1} respectively shift to 2855 and 2826 cm^{-1} in the rotator solid (S*I*). This shifting to higher frequencies is characteristic of the presence of gauche disorder in the alkyl chain. A change from a doublet to a single band is observed in the carboxylate asymmetric stretching band from the S*II* to S*I* phase, proving that changes in the coordination of the carboxylate group to the Pb(II) have taken place at this transition (Figure 5b). Moreover, the crystal field splitting observed when n > 9 in the CH_2 scissoring (around 1465 cm^{-1}) and rocking (around 720 cm^{-1}) modes also disappears at this temperature (Figure 5c). These facts, point to a polymorphic change to a more disordered solid (the *all-trans* carbon planes start to rotate) taking place at this temperature. In addition, very weak bands ascribed to localized *gtg* (*kink*) sequences at 1306 cm-^{1} and end gauche defects at about 1340 cm^{-1} can be observed. These bands correspond to kink defects appearing in the alkyl chain as consequence of methylene rotational movements taking place at the solid transition temperature.

Physical Chemistry Chemical Physics Accepted Manuscript

Please do not adjust margins

View Article Online
DOI: 10.1039/C7CP02351K

Published on 07 June 2017. Downloaded by State University of New York at Binghamton on 07/06/2017 16:49:10.

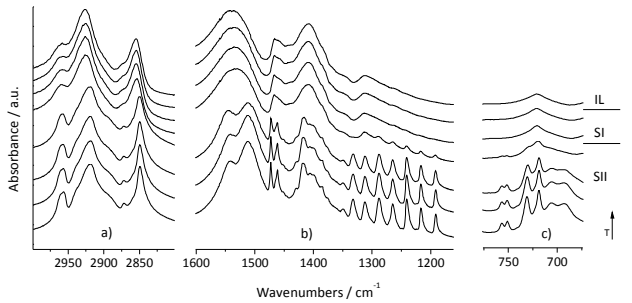

Fig. 5. FTIR spectra of $Pb(C14)_2$, at 298, 313, 333, 353, 368, 373, 378 and 393 K, showing the different phases (S*II*, S*I* and IL).

ssNMR confirms the results observed by FTIR. Overall, the C-13 spectra exhibit a line narrowing effect in all peaks due to an increase in chains mobility at the *SI* phase (see Figs S17, S19, S20 and S22 in Supp. Info.). One methyl (14.7 ppm) and carboxylate (184.7 ppm) are shown in the C-13 spectra in this phase for long-chain lead soaps, supporting the idea of the rotational motion of the alkyl chains. In addition, a high field shift (~0.4 ppm), from *SII* all *trans* chain conformations, of the methyl peak due to the *gauche* effect is observed, and in other carbons in the chain as well. The increased molecular mobility in the *SI* phase is also seen in the corresponding Pb-207 ssNMR spectra of $Pb(C10)_2$ and $Pb(C14)_2$ acquired at 364.9 and 379.5 K, respectively (see Figs S18 and S21, and Table S7 in Supp. Info.). In both cases, the spectral span, Ω, is reduced from about 700-677 ppm to 490-462 ppm. In addition, the increase in the value of δ_{iso} from ~-2130 ppm to ~-1550 could be attributed partly to a decrease in the mean Pb-O bond length.[52] The higher disorder and possible motion might affect to the ionic parts, and as it happens in shorter members of the lead soaps family, the conductivity increases considerably in the S*I* phase, in contrast with the crystal phase. FTIR, ssNMR and conductivity data for some members of the series are shown in the Supporting Information.

2- LC phase

This fluid phase is birefringent and shows a coherent order of stacking of layers (few peaks in diffraction). The liquid crystal phase has been well described,[9-13,16] and it corresponds to a smectic-A like (or *neat*) liquid crystal. This structure can be deduced from the fan-shaped domains studied by optical microscopy with crossed polars (see Figure 4).[10,16,53]

The molecules are grouped in layers and, then, in domains. The alkyl chains are "melted" (dynamical disorder of gauche defects), with the director vector perpendicular to the layers. Although the LC phase is fluid, PDF shows a similar order in the short range (up to 5-6 Å), revealing that the atoms (especially the heavy ones) are in the same environment and coordination as in the S*I* phase (Figure 3).

3- IL phase

The so-called "isotropic" liquid phase shows no birefringence and no peaks in diffraction. The phase is fluid and the alkyl chains are completely disordered (FTIR). However, there are not significant differences between the PDFs of the LC and the IL phases, indicating the same local order up to 10 Å, which rules out the existence of isolated $Pb(Cn)_2$ units. Therefore, the IL phase cannot be considered completely disordered and the difference between the LC and the IL phases could be due to the domain size, bigger in the case of the liquid crystal, so that the birefringence and also diffraction can be detected.

Conclusions

The family of lead(II) soaps, including in this work members from acetate to stearate (octadecanoate), has been fully analysed by means of calorimetry, diffraction and scattering, spectroscopy and other techniques. Four phases are present in these compounds: the crystal phase at room temperature, a solid mesophase, a liquid crystal and a liquid phase.

The crystal structure of the room temperature solid phase from octanoate to octadecanoate has been solved for the first time, finding two polymorphic forms for short and long-chain members and monotropic polymorphism for nonanoate and decanoate.

The solid intermediate phase, defined as rotator, is crystalline and shows some cooperative mobility in the alkyl chains. PDF-Analysis shows that the first Pb-Pb distance shrinks with respect to the crystal phase. A model for the structure of the Pb atoms is also given for this phase. The PDF curves show that this solid mesophase present a similar local structure in the very short range as the liquid crystal and the liquid, independently of the alkyl chain length.

PDF Analysis: a new technique to study lead soaps in Art.

The detection of lead soaps in artworks, as degradation products (*e.g.* $Pb(C16)_2$ and $Pb(C18)_2$), is mainly carried out by FTIR and other techniques like diffraction or electron microscopy. The vibrational frequencies or diffraction patterns used to identify lead soaps are those of the crystal phase. This poses an important limitation to the early detection of these salts during their initial formation, where nanocrystals or mesophases can be formed lacking long-range ordering.

The experiments carried out here on the members of the series in all their phases show that the PDF offers a unique signature of the local structure, very similar for all the lead soaps phases. This means that any lead soap can be identified using the PDF pattern as a *fingerprint*. In the particular case of *SII*, the PDF in the short range is obviously different for polymorphs A and B, but again similar for the same polymorphic form in different members of the series. The use of PDF analysis can therefore be of significant help significantly in the detection and the structural study of disordered as well as ordered phases of these systems. The sensitivity of the technique using X-rays is higher for high-Z atoms, which would favour the detection of lead soaps. In this sense, PDF Analysis or X-ray Absorption (XAS) using micro-sized beams are potential tools, complementary to the existing ones, that could be used on the detection of metal soaps in paintings, even in the initial stages of formation.

Physical Chemistry Chemical Physics Accepted Manuscript

This journal is © The Royal Society of Chemistry 20xx

Please do not adjust margins

View Article Online
DOI: 10.1039/C7CP02351K
PCCP ARTICLE

Published on 07 June 2017. Downloaded by State University of New York at Binghamton on 07/06/2017 16:49:10.

Physical Chemistry Chemical Physics Accepted Manuscript

Acknowledgements

Partial support of this research by the DGICYT of the Spanish "Ministerio de Educación y Ciencia" (Grants in aid for Scientific Research CTQ2008-06328, CTQ2013-41781-P and CTQ2015-67755-C2-1-R) is gratefully acknowledged. LG acknowledges financial support provided by CSIC. The authors wish to thank the beamlines BM25-Spline and ID31 (ESRF, Grenoble, France), I711 (Max II ring, MAX IV Laboratory, Lund, Sweden), the Center of Scientific Instrumentation at the University Complutense of Madrid (CAI of XRD, Centro de Asistencia a la Investigación), and the Laboratory for Crystallographic Studies (IACT, CSIC-UGR), and their staff, for the use of their technical facilities and help.

Notes and references

1 P. Franzosini and M. Sanesi, Eds. *Thermodynamic and Transport Properties of Organic Salts*; Pergamon Press: London, 1980.
2 D. R. MacFarlane, J. Huang and M. Forsyth, *Nature,* 1999, **402**, 792794.
3 K. Binnemans, *Chem. Rev*. 2005, **105**, 4148.
4 a) J. Adebahr, A. J. Seeber, D. R. MacFarlane and M. Forsyth, J. *Appl. Phys*. 2005, **97**, 093904; b) J. Adebahr, A. J. Seeber, D. R. MacFarlane and M. Forsyth, *J. Phys. Chem*. *B* 2005, **109**, 20087.
5 Q. Dai, D. R. MacFarlane, P. C. Howlett and M. Forsyth, *Angew. Chem.* 2005, **117**, 317.
6 C. G. Bazuin, D. Guillon, A. Skoulios, A. M. Amorim da Costa, H. D. Burrows, C. F. G. C. Geraldes, J. J. C. Teixeira-Dias, E. Blackmore and G. J. T. Tiddy, *Liq. Cryst.*, 1988, **3**, 1655.
7 J. Schwede, L. Koehler, H. P. Grossmann, M. Pietralla and H. D. Burrows, *Liq. Cryst.*, 1994, **16**, 267.
8 H. A. Ellis and J. W. C. de Vries, *Mol. Cryst. Liq. Cryst.*, 1988, **163**, 133.
9 A. M. Amorim da Costa, H. D. Burrows, C. F. C. G. Geraldes, J. J. C. Teixeira-Dias, C. G.; Bazuin, D. Guillon, A. Skoulios, E. Blackmore, G. J. T. Tiddy and D. L. Turner *Liq. Cryst*.**,** 1986, **1**, 215.
10 A. Sánchez Arenas, M. V. García Pérez, M. I. Redondo Yélamos, J. A. R. Cheda, M. V. Roux and C. Turrión, *Liq. Cryst.*, 1995, **18**, 431.
11 S. A. Adeosun and S. J. Sime, *Thermochim. Acta*, 1978, **27**, 319.
12 M. E. Ekwunife, M. U. Nwachukwu, F. P. Rinehart and S. Sime, *J. Chem. Soc. Faraday Trans. I*, 1975, **71**, 1432.
13 F. J. Martínez-Casado, M. V. García Pérez, M. I. Redondo Yélamos, J. A. R. Cheda, A. Sánchez Arenas, S. López de Andrés, J. García-Barriocanal, A. Rivera, C. León and J. Santamaría, *J. Phys. Chem. C*, 2007, **111**, 6826.
14 F. J. Martínez-Casado, A. Sánchez Arenas, M. V. García Pérez, M. I. Redondo Yélamos, S. López de Andrés and J. A. R. Cheda, *J. Chem. Therm.*, 2007, **39**, 455.
15 F. J. Martínez-Casado, M. Ramos Riesco, A. Sánchez Arenas, M. V. García Pérez, M. I. Redondo-Yélamos, S. López-Andrés, L. Garrido and J. A. R. Cheda, *J. Phys. Chem. B*, 2008, **112**, 16601.
16 F. J. Martínez-Casado, M. Ramos-Riesco, J. A. Rodríguez-Cheda, F. Cucinotta, A. Fernández-Martínez, L. Garrido, E. Matesanz and L. Marchese, *J. Mater. Chem. C*, 2014, **15**, 497.
17 F. J. Martínez-Casado, M. Ramos-Riesco, J. A. Rodríguez-Cheda, F. Cucinotta, E. Matesanz, I. Miletto, E. Gianotti and L. Marchese, *Inorg. Chem.* 2016, **55**, 8576.
18 F. J. Martínez-Casado, M. Ramos-Riesco, M. I. Redondo-Yélamos, A. Sánchez Arenas and J. A. R. Cheda, *J. Therm. Anal. Calorim.*, 2012, **108**, 399.
19 a) M. Ramos Riesco, F. J. Martínez-Casado, S. López-Andrés, M. V. García Pérez, M. I. Redondo-Yélamos, M. R. Torres, L. Garrido and J. A. R. Cheda, *Cryst. Growth Des.* 2008, **8**, 2547; b) M. Ramos Riesco, F. J. Martínez-Casado, J. A. Rodríguez Cheda, M. I. Redondo-Yélamos, A. Fernández-Martínez and S. López de Andrés, *Cryst. Growth Des.*, 2015, **15**, 497; c) M. Ramos Riesco, F. J. Martínez-Casado, J. A. Rodríguez-Cheda, M. I. Redondo-Yélamos, I. da Silva, T. Plivelic, S. López de Andrés and P. Ferloni, *Cryst. Growth Des.*, 2015, **15**, 2005.
20 F. J. Martínez-Casado, M. Ramos-Riesco, M. I. Redondo-Yélamos, D. Choquesillo-Lazarte, S. López-Andrés, J. A. Rodríguez -Cheda, *Cryst. Growth Des.*, 2011, **11**, 1021.
21 F. Lacouture, M. Francois, C. Didierjean, J. P. Rivera, E. Rocca and J. Steinmetza, *Acta Cryst.*, 2001. **C57**, 530.
22 F. J. Martínez-Casado, M. Ramos-Riesco, I. da Silva, M. I. Redondo-Yélamos, A. Labrador and J. A. R. Cheda, *Cryst. Growth Des.*, 2011, **11**, 759.
23 J. Catalano, A. Murphy, Y. Yao, G. P. A. Yap, N Zumbulyadis, S. A. Centeno and C Dybowski, *Dalton Trans.*, 2015, **44**, 2340.
24 a) W. C. De Gruijter and T. Bokx, *J. Solid State Chem.* 1973, **6**, 271; b) A. Strasser and A. Vogler, *Inorg. Chem. Comm.* 2004, **7**, 528; c) A. Strasser and A. Vogler, *J. Photochem. Photobiol., A* 2004, **165**, 165; d) Z.-H. Lei, X. Li and L.-N. Dong, *Inorg. Chem. Comm.* 2010, **13**, 1383; e) Q. Y. Liu and L. Xu, *Eur. J. Inorg. Chem.* 2006, **8**, 1620.
25 F. J. Martínez Casado, L. Cañadillas-Delgado, F. Cucinotta, A. Guerrero-Martínez, M. Ramos Riesco, L. Marchese and J. A. R. Cheda, *CrystEngComm*, 2012, **14**, 2660.
26 H. D. Burrows, *Mater. Lett.*, 1988, **6**, 191.
27 G. Klimusheva, T. Mirnaya, and Y. Garbovskiy *Liq. Cryst. Rev.*, 2015, **3**, 28.
28 V. Rudenko, Y. Garbovskiy, G. Klimusheva, T. Mirnaya, and G. Yaremchuk, *J. Opt. Soc. Am. B*, 2016, **33**, 648.
29 N. P. Middelkoop, J. Noble, J. Wadum and B. Broos.. *Rembrandt under the Scalpel: The Anatomy Lesson of Dr Nicolaes Tulp Dissected*. Amsterdam/The Hague. 1998.
30 J. J. Boon and E. S. B. Ferreira (Eds). *Reporting Highlights of the De Mayerne Programme*; The Hague, 2006.
31 J. J. Hermans, K. Keune, A. van Loon and P. D. Iedema, *Phys. Chem. Chem. Phys.*, 2016, **18**, 10896.
32 M. G. MacDonald, M. R. Palmer, M. R. Suchomel and B. H. Berrie, *ACS Omega*, 2016, **1**, 344–350
33 G. Osmond, J. J. Boon, L. Puskar and J. Drennan, *Appl. Spectroscop.,* 2016, **66**, 1136.
34 K. Keune, *Binding Medium, Pigments, and Metal Soaps Characterised and Localised in Paint Cross-sections*. PhD thesis, University of Amsterdam, 2005
35 S. A. Centeno and D. Mahon, *Metropol. Mus Art B.*, 2009, **67**, 12.
36 L. de Viguerie, P. A. Payard, E. Portero, Ph. Walter and M. Cotte *Prog. Org. Coat.,* 2016, **93**, 46.
37 L. Robinet and M. C. Corbeil, *Stud. Conser.*, 2003, **48**, 23.
38 J. J. Hermans, K. Keune, A. Van Loon, R. W. Corkery and P. D. Iedema, *RCS Adv.*, 2016, **6**, 93363.

Please do not adjust margins

View Article Online
DOI: 10.1039/C7CP02351K

39 G. M. Sheldrick, *Acta Cryst.*, 2008, **A64**, 112.
40 J. Rodríguez-Carvajal, *Physica B*, 1993, **192**, 55.
41 J. Rodriguez-Carvajal, *Commission on Powder Diffraction (IUCr). Newsletter*, 2001, **26**, 12-19.
42 P. J. Chupas, X. Y. Qiu, J. C. Hanson, P.L. Lee, C. P. Grey and S. J. L. Billinge, *J. Appl. Crystallogr.*, 2003, **36**, 1342.
43 a) A. P. Hammersley, S. O. Svensson, M. Hanfland, A. N. Fitch and D. Hausermann *High Press. Res.*, 1996, **14**, 235; b) Fit2D V9.129 Reference Manual V. 3.1; A. P. Hammersley, in *ESRF Internal Report*, ESRF98HA01T, 1998.
44 P. Juhás, T. Davis, C. L. Farrow and S. J. L. Billinge, *J. Appl. Cryst.*, 2013, **46**, 560.
45 J. R. Ascenso, R. K. Harris and P. Granger, *J. Organomet. Chem.* 1986, **301**, C23.
46 M. J. González-Tejera, S. López-Andrés, M. V. García, M. I. Redondo and J. A. Rodríguez Cheda, *J. Cryst. Growth*, 1995, **152**, 330.
47 J. Catalano, Y. Yao, A. Murphy, N. Zumbulyadis, S. A. Centeno and C. Dybowski, *Appl. Spectrosc.*, 2014, **68**, 280.
48 A. Boultif and D. Louër, *J. Appl. Cryst.*, 2004, **37**, 724.
49 C. L. Farrow, P. Juhás, J. W. Liu, D. Bryndin, E. S. Božin, J. Bloch, Th. Proffen and S. J. L. Billinge, *J. Phys.: Condens. Matter*, 2007, **19**, 335219.
50 A. E. Skoulios and V. Luzzati, *Acta Cryst.*, 1961, **14**, 278.
51 B. Gallot and A. E. Skoulios, *Acta Cryst.*, 1962, **15**, 826.
52 F. Fayon, I. Farnan, C. Bessada, J. Coutures, D. Massiot and J. P. Coutures. *J. Am. Chem. Soc.*, 1997, **119**, 6837.
53 a) F. J. Martínez-Casado, M. Ramos-Riesco and J. A. R. Cheda, *J. Therm. Anal. Calorim.*, 2007, **87**, 73; b) F. J. Martínez Casado, M. Ramos Riesco, I. da Silva, A. Labrador, M. I. Redondo, M. V. García Pérez, S. López-Andrés and J. A. R. Cheda, *J. Phys. Chem. B* 2010, **114**, 10075; c) F. J. Martínez Casado, M. Ramos Riesco, I. da Silva, M. I. Redondo, and J. A. R. Cheda, *RSC Adv.* 2011, **1**, 147.

Published on 07 June 2017. Downloaded by State University of New York at Binghamton on 07/06/2017 16:49:10.

Physical Chemistry Chemical Physics Accepted Manuscript

This journal is © The Royal Society of Chemistry 20xx

Please do not adjust margins

View Article Online
DOI: 10.1039/C7CP02351K

Published on 07 June 2017. Downloaded by State University of New York at Binghamton on 07/06/2017 16:49:10.

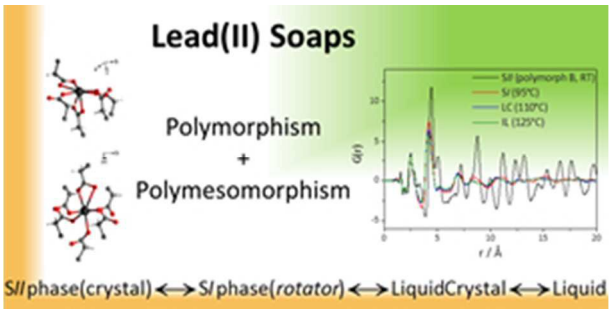

Physical Chemistry Chemical Physics Accepted Manuscript